

Article

Optimizing the Design of an Interior Permanent Magnet Synchronous Motor for Electric Vehicles with a Hybrid ABC-SVM Algorithm

Jong-Woon Park ¹, Min-Mo Koo ², Hyun-Uk Seo ³ and Dong-Kuk Lim ^{1,*}

¹ Department of Electrical, Electronic, and Computer Engineering, University of Ulsan, Ulsan 44610, Republic of Korea; woon8303@mail.ulsan.ac.kr

² Department of Automotive Materials & Components R&D Group, Korea Institute of Industrial Technology, Gwangju 61012, Republic of Korea; mmkoo@kitech.re.kr

³ Department of Robotics & Mechatronics, Korea Institute of Machinery and Materials, Daejeon 34103, Republic of Korea; shu@kimm.re.kr

* Correspondence: ldk8745@ulsan.ac.kr; Tel.: +82-52-259-1072

Abstract: This paper presents a comprehensive investigation of the optimal design of an interior permanent magnet synchronous motor (IPMSM) for electric vehicles (EVs), utilizing the hybrid artificial bee colony algorithm–support vector machine (HAS) algorithm. The performance of the drive motor is a crucial determinant of the overall vehicle performance, particularly in EVs that rely solely on a motor for propulsion. In this context, interior permanent magnet synchronous motors (IPMSMs) offer a compelling choice due to their high torque density, wide speed range, superior efficiency, and robustness. However, accurate analysis of the nonlinear characteristics of IPMSMs necessitates finite element analysis, which can be time-consuming. Therefore, research into methods for deriving an optimal model with minimal computation is of significant importance. The HAS is a powerful multimodal optimization technique that is capable of exploring several optimal solutions. It enhances the navigation capability by combining the artificial bee colony algorithm (ABC) with the kernel support vector machine (KSVM). Specifically, the algorithm improves the search ability by optimizing the movement of bees in each region generated by the KSVM. Furthermore, hybridization with the Nelder–Mead method ensures accurate and quick convergence at pointers discovered in the ABC. To demonstrate the effectiveness of the proposed algorithm, this study compared its performance with a conventional algorithm in two mathematical test functions, verifying its remarkable performance. Finally, the HAS algorithm was applied to the optimal design of the IPMSM for EVs. Overall, this paper provides a thorough investigation of the application of the HAS algorithm to the design of IPMSMs for electric vehicles, and its application is expected to benefit from the combination of machine-learning techniques with various other optimization algorithms.



Citation: Park, J.-W.; Koo, M.-M.; Seo, H.-U.; Lim, D.-K. Optimizing the Design of an Interior Permanent Magnet Synchronous Motor for Electric Vehicles with a Hybrid ABC-SVM Algorithm. *Energies* **2023**, *16*, 5087. <https://doi.org/10.3390/en16135087>

Academic Editors: Giovanni Lutzemberger, Guang-Jin Li and Xiao Chen

Received: 18 May 2023

Revised: 17 June 2023

Accepted: 29 June 2023

Published: 30 June 2023



Copyright: © 2023 by the authors. Licensee MDPI, Basel, Switzerland. This article is an open access article distributed under the terms and conditions of the Creative Commons Attribution (CC BY) license (<https://creativecommons.org/licenses/by/4.0/>).

1. Introduction

Recently, the paradigm of the automobile industry has focused on resolving various environmental regulations and improving the fuel efficiency of automobiles. Accordingly, research and development and the commercialization of eco-friendly energy-based vehicles, such as electric vehicles (EVs), are spreading worldwide.

The performance of the drive motor is an important measure of the performance of the vehicle because EVs drive using only a motor and not an engine [1]. In this regard, interior permanent magnet synchronous motors (IPMSMs) are considered an appealing alternative due to their numerous benefits, such as high torque density, wide speed range, good efficiency, and robustness [2,3]. However, in the case of IPMSMs, permanent magnets

are inserted into the rotor, and harmonics are included in the magnetic flux in the air gap, causing vibration and noise [4,5]. There are two categories of torque ripple minimization schemes to solve this problem: design-oriented and control-oriented approaches [6]. In this paper, the torque ripple was reduced by using a design-oriented approach to optimize the design parameters of the rotor in IPMSMs.

Due to the nonlinear magnetic saturation characteristics of an electric motor, finite element analysis (FEA) is necessary to accurately analyze the electromagnetic characteristics of the motor [7]. However, the computational cost problem of FEA becomes worse when it is applied to a multimodal optimization problem, such as the optimal design of the motor [8]. Therefore, various optimization algorithms have been investigated to solve this problem. Optimization algorithms have been the subject of extensive research, leading to the development and refinement of a wide array of techniques. These span from traditional methods such as gradient descent and Newton's method to contemporary heuristic-based algorithms, including genetic algorithms, particle swarm optimization, and artificial bee colony (ABC) algorithm. Each method possesses unique strengths and weaknesses, and their suitability is contingent upon the specific attributes of the problem under consideration [9].

Despite the extensive research in this area, there remains a need for an optimization algorithm that can effectively handle the computational cost constraints inherent in the design optimization of electric motors [10,11]. Therefore, this paper proposes a hybrid artificial bee colony–support vector machine algorithm (HAS) for overcoming computational cost constraints. The HAS is a multimodal optimization algorithm that combines the conventional ABC algorithm with the kernel support vector machine (KSVM), which is a classification technique of machine learning. The behavior of each bee in the ABC is varied by utilizing the three regions formed by the KSVM. Furthermore, the convergence performance of the algorithm is improved by combining the Nelder–Mead method (NM), which is a deterministic method.

Two mathematical test functions with numerous local peaks were applied to the HAS, and its outstanding performance was confirmed by comparison to the conventional ABC and niching genetic algorithm (NGA). The proposed algorithm was applied to the design optimization of an IPMSM for EVs in order to derive an optimal design that minimizes torque ripple. Finally, to confirm the performance and stability of the model designed through the HAS, irreversible demagnetization analysis under high-temperature conditions and stress analysis under high-speed operation was performed. Through this, the validity of the model proposed in this paper was confirmed.

2. Proposed Algorithm

Even though the conventional ABC performs better in multimodal optimization problems than other heuristic algorithms, the ABC also has a problem that requires many function calls to converge to an accurate peak like other stochastic algorithms. To address the problem with computational cost, the HAS is proposed. The HAS improves the performance of the conventional ABC by using the KSVM and the NM.

2.1. Latin Hypercube Sampling

Latin hypercube sampling (LHS) is a statistical method for generating samples from a multivariate distribution [12]. This process is visually represented in Figure 1. Here, the domain is divided into N equal intervals, with a sample randomly selected from each, creating a uniform distribution across the domain. The parameter N is adjustable based on problem complexity, computational resources, and desired accuracy. While there is no theoretical upper limit to N , practical constraints such as computational time and memory exist. As N increases, sampling precision improves but at the cost of computational resources. The optimal N value is problem-specific and determined experimentally. LHS allows for a representative sample set without a large number of samples, providing

comprehensive sampling which is especially beneficial in high-dimensional or nonlinear problems where random sampling may be inadequate.

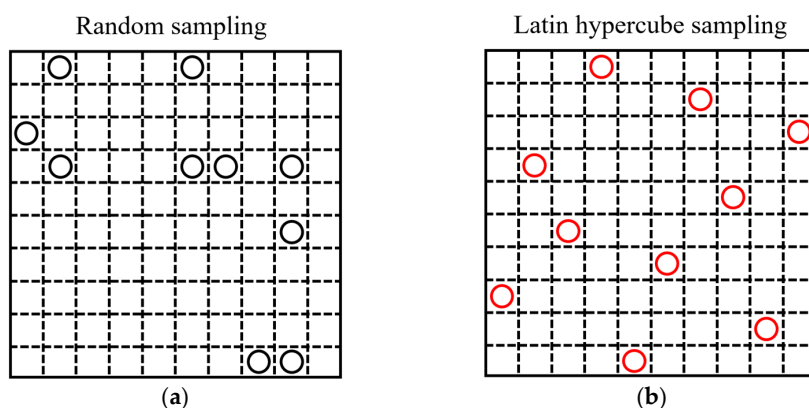


Figure 1. The comparison sampling: (a) Random sampling; (b) Latin hypercube sampling.

2.2. Conventional Artificial Colony Bee Algorithm

The concept of the ABC was derived from honeybees' clever foraging behavior to find suitable solutions to optimization problems [13]. The ABC consists of three types of bees: an employed bee, an onlooker bee, and a scouting bee [14]. Employed bees find a suitable solution, onlooker bees utilize other bee data to speed up convergence, and scouting bees improve the capability to eliminate local optima.

The employed bee computes the suitability of the assigned and neighboring sources and presents the source with greater suitability to the onlooker bees. The employed bee moves toward the nearby optimal solution as follows:

$$v_{ik} = x_{ik} + Acc \cdot r \cdot (x_{ik} - x_{jk}) \quad (1)$$

where v_{ik} indicates the neighboring source of the source assigned to it, while x_{ik} represents the source assigned to it. x_{jk} is a random source picked from among all sources, save those designated to x_{ik} , and r is a random number in $[-1, 1]$. Additionally, Acc is the acceleration factor, which is fixed as a constant. As a result, the convergence performance around sources can be degraded. To solve this problem, the HAS proposed in this paper leverages the region generated through the KSVM. This allows for an adaptive Acc value that varies in response to the objective function, thereby enhancing the algorithm's performance.

2.3. Kernel Support Vector Machine

The support vector machine (SVM) is a supervised learning model technique that is utilized in domains such as pattern identification and data analysis [15,16]. However, the SVM is a linear classification model, so it is difficult to use it to solve a problem that calls for nonlinear separation. This problem was resolved by the development of a KSVM with a kernel trick applied to an SVM. The KSVM is a technique for obtaining a separation interface at an existing dimension through linear separation using the SVM after mapping data in a high dimension using a kernel trick [17].

The KSVM has two training parameters: the optimal cost parameter and the Gaussian kernel function parameter [17]. The cost parameter determines how many data samples are allowed to be placed in different classes.

The Gaussian kernel function parameter is related to the standard deviation of the Gaussian function, so it determines the distance that a data sample affects. In this paper, the HAS generates two regions for the top N% sample data by tuning the KSVM parameters. Figure 2a,b show regions of the KSVM generated using the sample data of the ABC. As the training data increase as the algorithm iterates, the region around the optimal point is clearly created during the convergence iteration. Regions created by the HAS utilizing the KSVM are used to improve the navigation performance of the ABC.

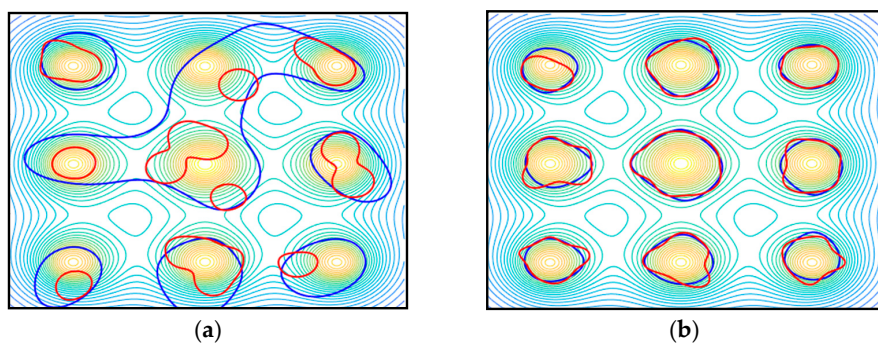


Figure 2. Regions created by the KSVM using sample data: (a) Initial iteration of the algorithm; (b) Convergence iteration of the algorithm.

2.4. Enhanced Artificial Colony Bee Algorithm

The HAS proposed in this paper improves the navigation performance of bees in each area created through the KSVM, as shown in Figure 3. The sections below provide a description of each region.

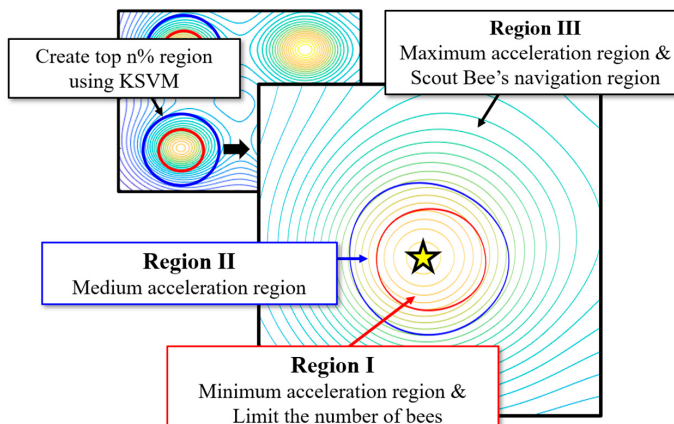


Figure 3. Segmenting regions schematic diagram of the HAS.

2.4.1. Convergence Region (Region I)

Since the convergence region is located closest to the peak, the HAS reduces the acceleration factor in (1), minimizing the distance between bees to improve the convergence performance. The acceleration factor in the convergence region is as follows:

$$Acc_i = R[(Acc \cdot f_{obj,i} \cdot N) / \sum_{n=1}^N f_{obj,n}] \quad (2)$$

where R is a random number in $[0.1, 0.9]$, $f_{obj,i}$ is the objective function value of the i_{th} sample, N is the total number of samples, and $f_{obj,n}$ is the objective function value of each sample. The acceleration coefficient Acc_i of the i_{th} sample is determined by considering the objective function values of other samples, as shown in (2). In addition, to prevent bee saturation in one region, the number of bees were limited so that they could explore various regions.

2.4.2. Detailed Navigation Region (Region II)

The detailed navigation region is formed widely around the peak, as shown in Figure 2. Samples within this region are highly likely to move to a nearby peak in the next iteration, so they need to have an appropriate acceleration factor. Therefore, the method for calculating the acceleration coefficient of the area is similar to (2); however, as shown in Table 1, R is a random variable in the range $[1.0, 1.5]$, which can speed up the honeybees' movement.

Table 1. Random number range for each region.

Regions	Random Number
Convergence region	0.1~0.9
Detailed navigation region	1.0~1.5
Exploration region	1.6~2.0

2.4.3. Exploration Region (Region III)

The exploration region refers to the remaining region, except for the region formed by the KSVM. Bees in this region have the highest acceleration coefficient to expand the search space and search for new peak points. Therefore, the method for obtaining the acceleration factor of the corresponding region is the same as that of other regions, but the range of the random variable R is a random variable with a range of [1.6, 2.0], as shown in Table 1, and the region is searched at the fastest speed. In addition, it becomes a new search space for bees and scouting bees that have moved out of the convergence area, so that the diversity of solutions can be secured.

2.5. Improved Nelder–Mead Method

The NM is a numerical method used to find the minimum or maximum of an objective function in a multidimensional space. It is a deterministic method based on function comparison and is often applied to nonlinear optimization problems for which derivatives may not be known [18]. However, it has the disadvantage of being able to converge to a nonstationary point for problems that can be solved by alternative methods [19,20]. Figure 4 shows the concept of the NM. It is designed to perform reflection, expansion, contraction, and shrinking operations repeatedly for the simplex to discover the optimal value in the n -dimensional space represented by the objective function. The NM is sensitive to the initial conditions, meaning that the algorithm's performance can be heavily influenced by the starting point. This can result in poor performance or becoming stuck in a suboptimal solution if the initial conditions are not carefully chosen. Therefore, in this paper, the search spaces of reflection and expansion were limited in consideration of the convergence region of the KSVM, as shown in Figure 4c,d, in order to prevent the searching of unnecessary points. If a sample goes out of bounds, it is placed on the outermost edge in the same direction within the region. Furthermore, the simplex in the HAS uses the sample data from the ABC to reduce computational cost constraints, thereby improving the accuracy of the optimal solution for each region during the convergence phase.

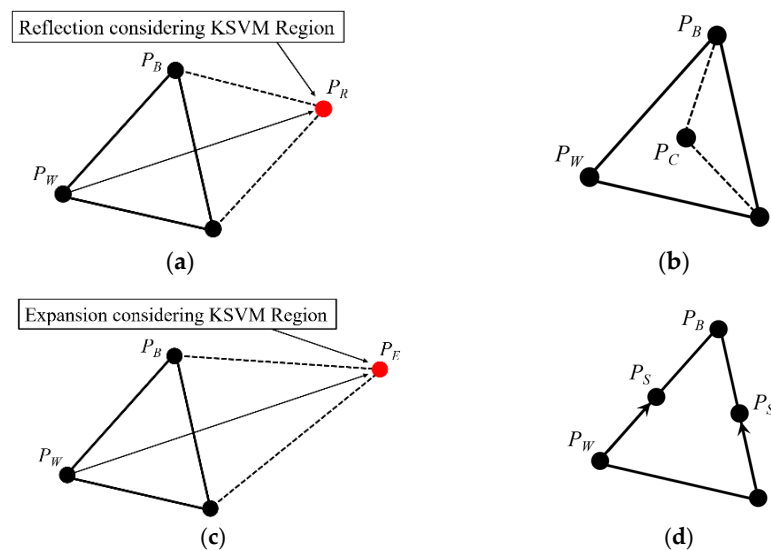


Figure 4. Nelder–Mead method conceptual diagram: (a) Reflection; (b) Contraction; (c) Expansion; (d) Shrinking.

2.6. Flow Chart of the HAS

The flow chart of the HAS is shown in Figure 5. The specific process of the proposed algorithm is as follows.

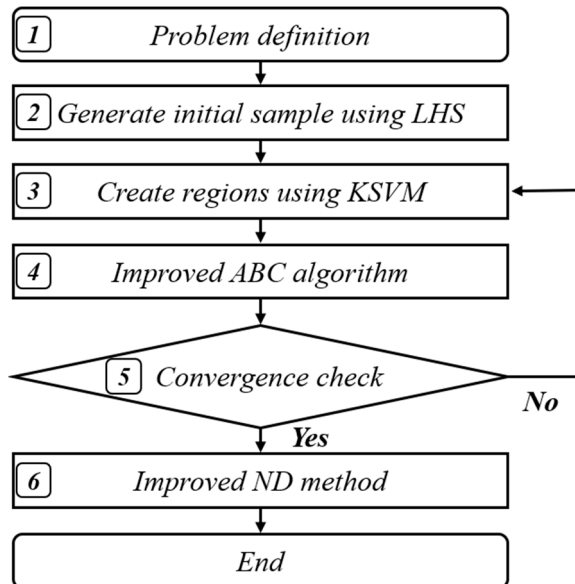


Figure 5. Flow chart of the HAS.

1. Problem definition: set the initial parameters of the objective function, the limiting condition, and the algorithm.
2. Generate initial sample using LHS: A set of initial samples are generated across the domain of the objective function. All samples are generated through LHS.
3. Create regions using the KSVM: The optimization process employs the use of the KSVM to generate a region for the samples in the objective function. This region is determined based on the objective value of the samples, and it is restricted to the top N% of the samples. As the optimization process continues, the acquired data are persistently retained, leading to a continual improvement in the performance of the employed optimization technique.
4. Improved ABC algorithm: Each bee is assigned a unique acceleration factor that determines its movement pattern within three distinct regions of the search space. As the bees explore the space, they continually record their movement data, which are then utilized to update the defined search space in subsequent iterations.
5. Convergence check: If there is no change in the searched peak for three iterations, the HAS is terminated. Otherwise, the process returns to step 3 to create a new region using the KSVM.
6. Improved ND method: The ND is executed by utilizing the optimal sample within the convergence region. The reflection and dilation steps are executed in terms of the convergence rate by considering the specific region.

2.7. Verification of the Algorithm

The efficacy of the proposed algorithm is assessed by applying it, along with the conventional ABC and NGA, to two test functions with 9 and 16 peak points, respectively. The results of this analysis serve to validate the performance of the proposed algorithm. The test functions are as follows:

$$f(x, y) = \sum_{i=1}^P \frac{m_i}{1 + [(x - x_i)^2 + (y - y_i)^2]/n_i} \quad (3)$$

Here, the performance of the proposed algorithm was evaluated using two test functions with different P , which are peak points as shown in Figure 6a,b. The magnitude of each peak point was determined by the parameters m_i and n_i , and the coordinates of the optimal points were represented by x_i and y_i . The optimization process was performed 100 times for each algorithm, and the success rate was calculated as the ratio of the number of peak points found over the total number of peaks. The results of the tests are presented in Table 2. The HAS, when combined with the improved NM, exhibits a significant improvement in success rates over the traditional ABC. Moreover, the HAS outperforms the ABC in terms of the number of function calls, as it effectively relocates samples using the KSVM. In conclusion, when compared to the conventional ABC and NGA on two test functions, the HAS demonstrates superior performance in both accuracy and computational cost.

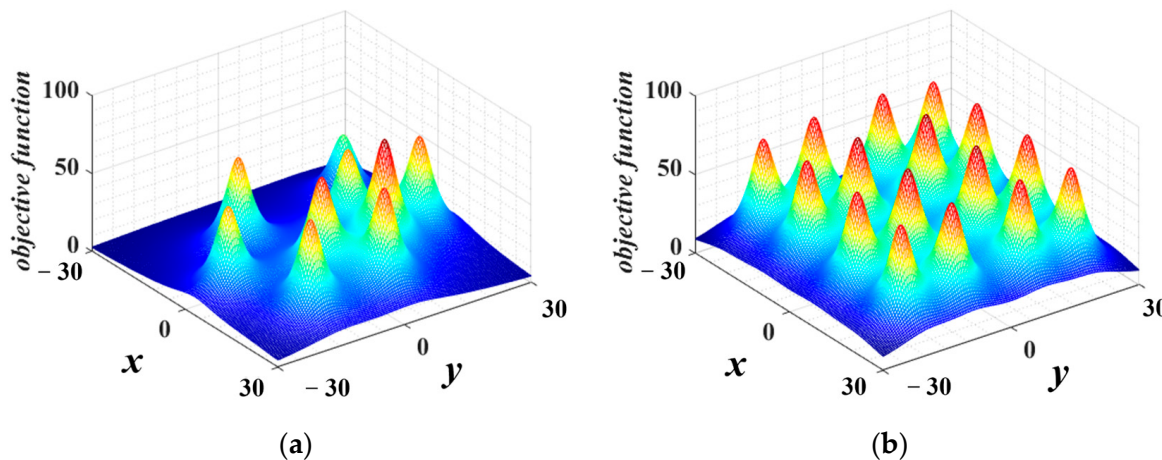


Figure 6. Plot of test functions: (a) Test function 1 with 9 peaks; (b) Test function 2 with 16 peaks.

Table 2. Optimization result.

Test function 1 (9 peaks)	ABC	NGA	HAS
Function calls	1105	1295	1030
Success rate [%]	83.55	77.78	97.13
Test function 2 (16 peaks)	ABC	NGA	HAS
Function calls	2100	1850	1765
Success rate [%]	84.88	81.56	96.01

3. Optimal Design and Performance Verification of IPMSM for EVs

In this section, the HAS, which has proven good performance in the previous section, is employed to optimize the configuration of the IPMSM. The optimization process aims to minimize torque ripple, taking into account factors such as torque and cogging torque. Each sample in the process carries design variable data, and FEA is performed each time the sample moves to a new coordinate. This iterative approach, facilitated by the HAS, enables continuous design improvements while performing fewer FEA analyses. Furthermore, to validate the design efficacy of the resulting optimal model, a multiphysics analysis which includes three analyses is conducted. This analysis serves to confirm the structural stability of the optimized model, thereby ensuring its practical viability.

3.1. IPMSM Design Objectives for EV Drive

In this paper, the focus is on optimizing an IPMSM-type permanent magnet motor for EVs, with a capacity of 80 kW. The design objectives of the motor are presented in Figure 7 and are aimed at achieving a maximum rated performance of 80 kW at 2850 RPM and continuous operation performance of 65 kW at 4400 RPM. The target performance is >95% efficiency, and the maximum operating speed of the motor is 12,000 RPM.

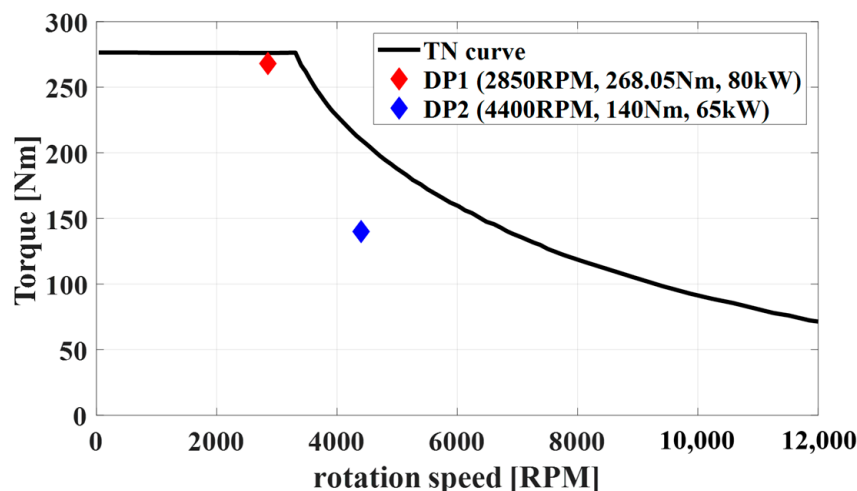


Figure 7. Target specification for motor for EV drive.

3.2. Analysis and Design Variables

The proposed algorithm was applied to the optimal design of the IPMSM for EVs, as depicted in Figure 8, to verify its applicability in practical electric motor design. The no-load and load conditions of the designed motor were analyzed using the commercial finite element analysis (FEA) tool, JMAG. The specifications and requirements of the motor are presented in Table 3.

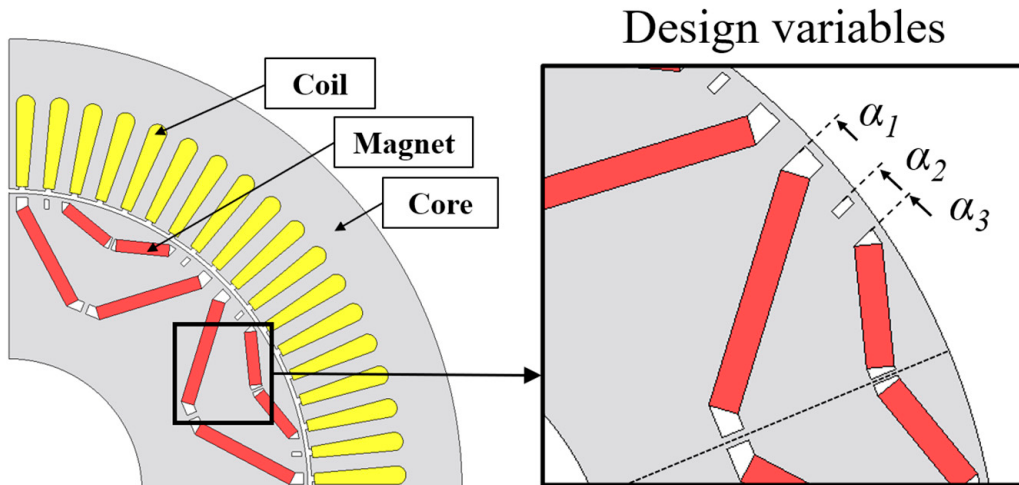


Figure 8. The benchmarked model for EVs.

Table 3. Specifications and requirements.

Parameter	Value
Pole/slot	8/72
Stator inner/outer diameter	133.6/200 [mm]
Rotor inner/outer diameter	50/132 [mm]
Stacking length	122.2 [mm]
Air gap	0.8 [mm]
Rated power/torque	80 [kW]/268.05 [Nm]
Rated speed/maximum speed	2850/12,000 [RPM]
Stator and rotor core material	27PNX1350F
Permanent magnet	N42UH-R ($Br_{min} = 1.29$ T)
Young's modulus (core/magnet)	200/150 [GPa]
Poisson's ratio (core/magnet)	0.3/0.3

In electric vehicles, both the torque ripple and cogging torque can negatively impact performance and efficiency, as well as contribute to increased wear and tear on motors and components. Additionally, these issues can reduce the performance range, battery life, and overall vehicle efficiency [5,21]. To solve this problem, the objective function of the algorithm was set to be torque ripple minimization. Additionally, since the shape of the motor affects several significant aspects of performance, the results will consider the average torque, torque ripple, efficiency, and other factors simultaneously.

Achieving optimal design requires variable selection and restriction conditions to be set. Through a design variable influence analysis [22], the hole gap between the magnet layer and the bridge, as illustrated in Figure 8, was identified as a key factor that significantly impacts the torque ripple, electromotive force, total harmonic distortion, and cogging torque. In addition, it was confirmed that the initial model, which was based on experimental data from [22], was nearly consistent with the simulation data. Therefore, three variables were altered in this optimal design, with all materials and structural variables of the initial model being strictly controlled. The design variables are defined as follows:

$$\begin{aligned}\alpha_3 &= \alpha_3 \\ \alpha_2 &= \alpha_3 + \text{difference} \\ \alpha_1 &= \alpha_2 + \text{difference}\end{aligned}\quad (4)$$

where α_1 , α_2 , and α_3 represent the pole-arc-to-pole pitch of the first-layer magnet, the hole gap, and the second-layer magnet, respectively. The pole-arc-to-pole pitch is a ratio that represents the relationship between the width of the magnetic pole, known as the pole arc, and the distance between identical points on two adjacent poles, referred to as the pole pitch. Each variable was constrained within a range that allows for practical design, ensuring that the proposed algorithm could yield a feasible design.

3.3. Optimal Design of IPMSM by Exploiting the HAS

The proposed algorithm is applied to the optimal design of an IPMSM. The objective function of the optimization is the torque ripple. Each sample has design variable data, and FEA analysis is executed each time it moves to a new coordinate.

Table 4 presents a summary of the optimization results and the performance of the initial model and the optimal models using the HAS. Model 1 exhibits the lowest torque ripple of 5.83%, which represents a significant improvement of 36.90% compared to the initial model. Furthermore, the average torque increased by 0.96% and the cogging torque decreased by 80.37%. In both Model 2 and Model 3, the torque ripple was reduced by 16.34% and 7.14%, respectively; based on this result, the performance of the algorithm could be verified. However, considering both the cogging torque and the average torque, it can be concluded that Model 1 is the optimal model. Figure 9a,b are the rotor shapes of the initial and optimal models, and Figure 10a,b show the torque and cogging torque pulsation of the initial and optimal models. Figure 11 shows the flux density distribution of the optimal design model, confirming that the maximum flux density is 2.1 T.

Table 4. Optimization results.

Model	Initial	Model 1	Model 2	Model 3
α_1 [%]	84.00	78.99	80.16	81.06
α_2 [%]	74.00	68.54	69.19	69.59
α_3 [%]	59.00	58.11	58.21	58.10
Torque ripple [%]	9.24	5.83	7.73	8.58
Average torque [Nm]	271.33	273.94	273.64	273.54
Cogging torque [Nm]	6.47	1.27	3.17	5.26
Efficiency [%]	95.69	95.73	95.73	95.73

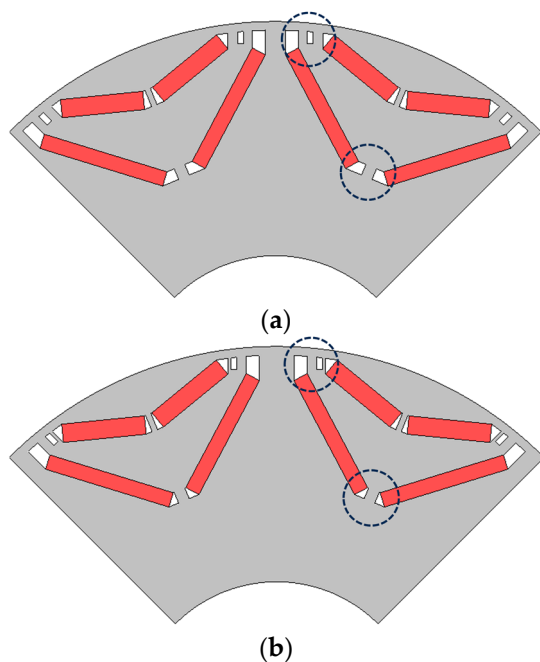


Figure 9. The rotor shape of IPMSMPM: (a) Initial model; (b) Optimal model.

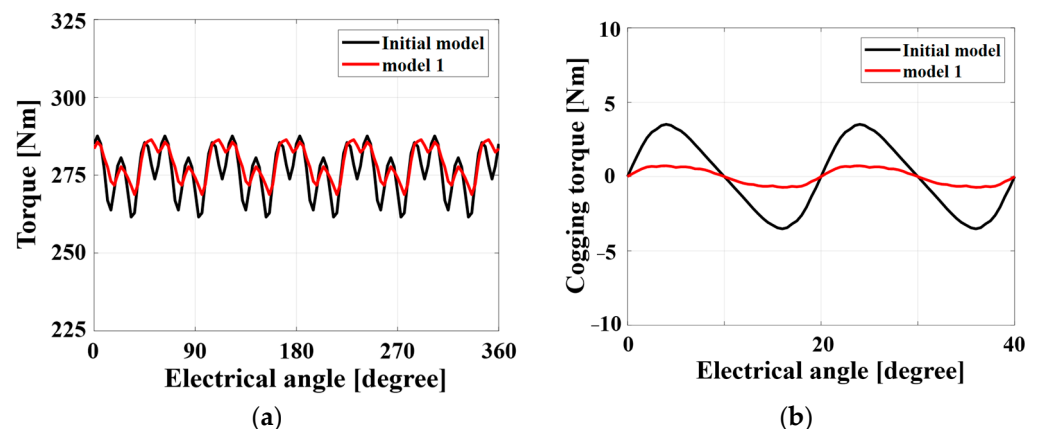


Figure 10. A waveform comparison of the initial model and optimal model: (a) Average torque; (b) Cogging torque.

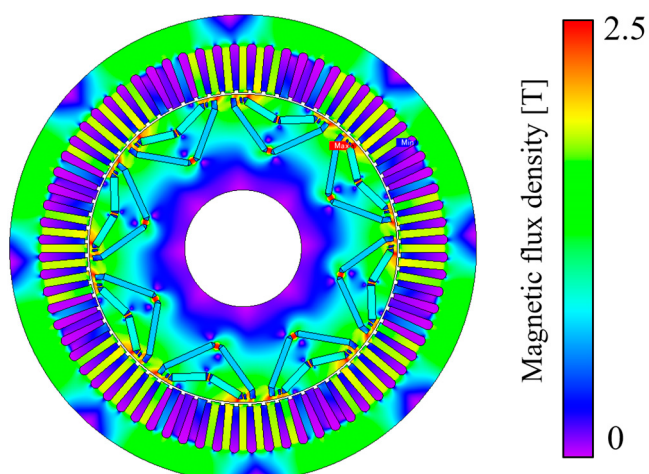


Figure 11. Magnetic flux density contour of the optimal model.

3.4. Validation of the Optimal Model by Multiphysics Analysis

Optimizing the design of an IPMSM necessitates a comprehensive multiphysics analysis for validation. This process encompasses critical stress and thermal evaluations, which are instrumental in ensuring the motor's robust performance and stability.

Given the wide speed range of the IPMSM, potential structural damage due to centrifugal forces at high speeds is a significant concern. To address this, a stress analysis is performed to affirm the structural integrity of the motor under such conditions [23,24]. Furthermore, maintaining thermal stability is of paramount importance, particularly with the use of neodymium permanent magnets. A thermal analysis is conducted to ascertain the capability of the motor to sustain optimal performance without succumbing to overheating or magnet demagnetization [25,26].

Therefore, this section carries out a multiphysics analysis process, which includes stress analysis, thermal analysis, and irreversible element analysis. These analyses are conducted to validate the structural stability of the optimized design. This comprehensive approach ensures the stability of the optimized IPMSM design, underpinning its practical viability and robustness.

3.4.1. Stress Analysis

Permanent magnets, i.e., the main material of IPMSMs for high-speed electric vehicles, have low tensile strength and have difficulties withstanding inertial forces under high acceleration. This can cause damage if surface-mounting structures are used, posing a major risk to motor stability [24,25]. Therefore, it is necessary to evaluate the stress distribution of the mover structure to ensure safety and reliability.

For motors with rotor-embedded magnets, the center post and bridges, which are most prone to breakage during high-speed operation, experience the maximum mechanical stress [27]. Therefore, to verify the stability of the optimal model, a stress analysis was performed at 13,200 RPM, which is 10% higher than the target maximum motor speed of 12,000 RPM specified in this paper. As shown in Figure 12, the stress at the center post between the magnets was the largest at about 380 MPa, but it was found that the stresses in the optimal rotor design did not exceed the yield strength of 27PNX1350, which has a yield strength of 420 MPa. This signifies that the optimal design, derived from the algorithm proposed in this study, possesses structural integrity and is capable of withstanding operational loads.

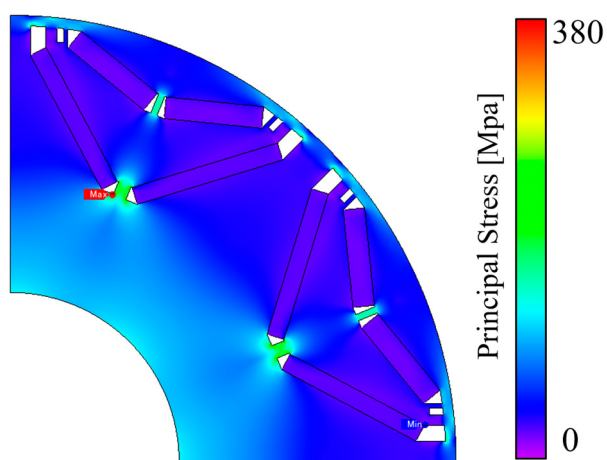


Figure 12. Stress analysis results at the maximum speed (13,200 RPM).

3.4.2. Thermal Analysis

In the design of IPMSMs, the thermal aspect is a crucial consideration due to the temperature-sensitive materials used in the motor. These materials, such as NdFeB magnets, have a temperature-dependent knee-point that can cause irreversible demagnetization at high temperatures [25]. To ensure the proper functioning of an IPMSM, it is essential to

accurately predict the permanent magnet temperature and maintain it within the desired range, while also ensuring that the overall temperature remains within acceptable levels.

Therefore, in this paper, the thermal characteristics at the continuous operating point were analyzed through a thermal equivalent circuit. The cooling method applied is an indirect cooling system using a water jacket with cooling water of EGW50/50, and the inlet temperature was set at 70 °C with a flow rate of 6 L per minute. The operating time was set to 2 h, and the thermal characteristic curve is shown in Figure 13 and Table 5. The designed model demonstrated thermal stability, with the highest temperature of the winding wire reaching 127.25 °C, while the other parts remained below 100 °C. Based on these results, it can be concluded that the designed model is reasonable and suitable for practical applications.

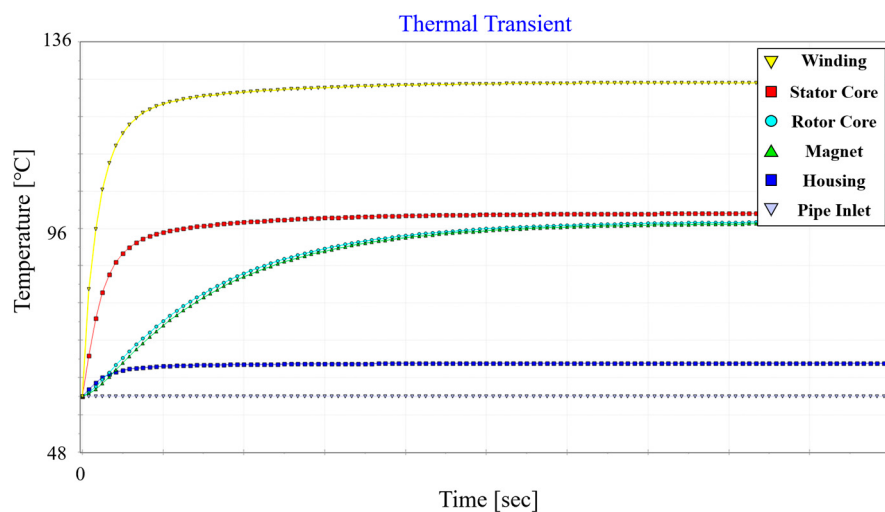


Figure 13. Graph of the thermal properties for each part.

Table 5. Results of thermal analysis for each part.

Part	Maximum Temperature [°C]
Winding	127.25
Stator core	99.20
Magnet	96.20
Rotor core	97.42
Housing	67.05

3.4.3. Permanent Magnet Irreversible Demagnetization Analysis

Irreversible demagnetization can occur in the permanent magnets used in IPMSMs when the electrical machine is overloaded or a short circuit occurs, due to the combined effect of magnetic field and temperature changes [26]. To accurately evaluate the demagnetization behavior, it is desirable to perform transient FEA of the performance of permanent magnets under harsh conditions. Therefore, in this paper, the stability of the motor was verified through demagnetization analysis based on the temperature data derived through the thermal equivalent circuit.

Thermal analysis showed that the stator reached a maximum temperature of 127.25 °C during continuous operation for 2 h. As the motor temperature may vary with the operating conditions, this paper evaluated the demagnetization of the permanent magnet at 150 °C. In addition, the d-axis control, which can apply the maximum magnetic field to the permanent magnet, was performed, and the back electromotive force (BEMF) was analyzed after performing no-load and severe load analyses, as shown in Figure 14a. As a result, as shown in Figure 14b, the difference between the maximum BEMF of the first stage and the maximum reversal force of the third stage was about 0.3%, proving that the motor designed in this paper is safe from the demagnetization of the permanent magnet.

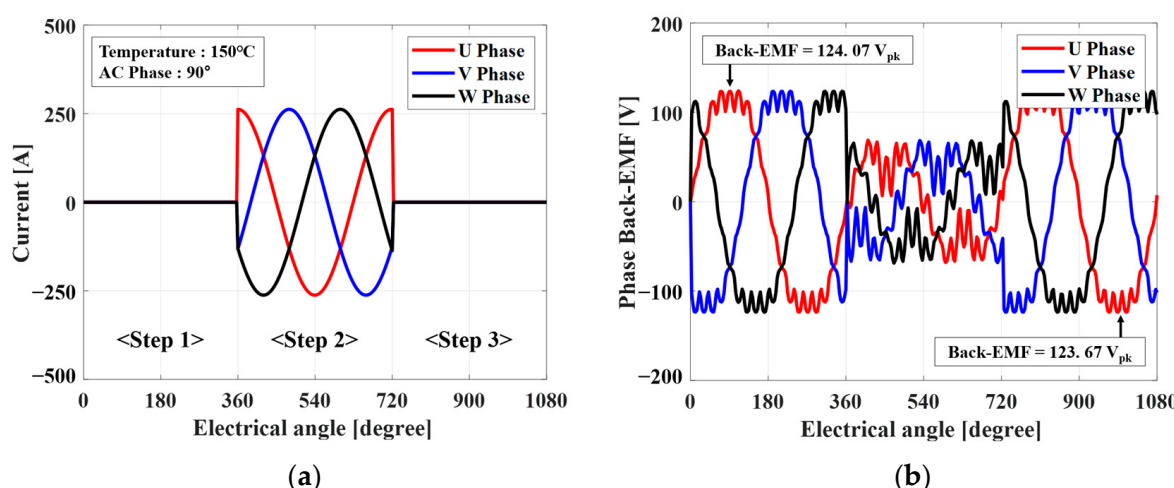


Figure 14. Results of the permanent magnet demagnetization analysis: (a) Applied current graph under harsh conditions (three steps); (b) Back EMF waveform graph.

4. Conclusions

This paper proposed a novel hybrid algorithm that reduces function calls while increasing accuracy for multimodal problems. The superior performance of the HAS, which utilized the region generated through the KSVM, was verified in mathematical test functions compared to the conventional ABC. The proposed method was successfully applied to optimize the design of IPMSMs, resulting in an optimal model with a torque ripple reduction rate of 36.90%. Moreover, the average torque increased by 0.96%, and the cogging torque decreased by 80.37% in this study. Finally, comprehensive stress, heat, and demagnetization analyses were conducted to ensure the optimized design's stability and reliability. These analyses are pivotal in confirming the designed model's structural integrity and thermal stability, ensuring its practical viability and application robustness. The results of this study are expected to have a wide range of applications in solving multimode optimization problems in various electrical devices using finite element analysis.

Author Contributions: Investigation, J.-W.P.; writing—original draft preparation, J.-W.P.; writing—review and editing, M.-M.K., H.-U.S. and D.-K.L. All authors have read and agreed to the published version of the manuscript.

Funding: This research received no external funding.

Data Availability Statement: Data is contained within the article.

Acknowledgments: This research was supported by “Regional Innovation Strategy (RIS)” through the National Research Foundation of Korea (NRF) funded by the Ministry of Education (MOE) (2021RIS-003), and by the National Research Foundation of Korea (NRF) grant supported by the Korea government (MSIT) (No. 2022R1A2C2092905).

Conflicts of Interest: The authors declare no conflict of interest.

References

1. Han, W.S. Optimal Design of EV Traction Motor with Cumulative Data Based Global Simplex Optimization Algorithm. Ph.D. Thesis, Sungkyunkwan University, Seoul, Republic of Korea, 2019.
2. Lee, S.K.; Kang, G.H.; Hur, J. Finite Element Computation of Magnetic Vibration Sources in 100 kW Two Fractional-Slot Interior Permanent Magnet Machines for Ship. *IEEE Trans. Magn.* **2012**, *48*, 867–870. [[CrossRef](#)]
3. Jiang, F.; Yang, F.; Sun, S.; Yang, K. Improved Linear Active Disturbance Rejection Control for IPMSM Drives Considering Load Inertia Mismatch. *Energies* **2022**, *15*, 1169. [[CrossRef](#)]
4. Song, C.H.; Kim, D.H.; Kim, K.C. Design of a Novel IPMSM Bridge for Torque Ripple Reduction. *IEEE Trans. Magn.* **2021**, *57*, 1–4. [[CrossRef](#)]
5. Kim, K.C. A Novel Method for Minimization of Cogging Torque and Torque Ripple for Interior Permanent Magnet Synchronous Motor. *IEEE Trans. Magn.* **2014**, *50*, 793–796. [[CrossRef](#)]

6. Cho, H.J.; Kwon, Y.C.; Sul, S.K. Torque Ripple-Minimizing Control of IPMSM With Optimized Current Trajectory. *IEEE Trans. Ind. Appl.* **2021**, *57*, 3852–3862. [[CrossRef](#)]
7. Caruso, M.; Tommaso, A.O.D.; Ferraris, L.; Miceli, R.; Viola, F. Finite-element performance comparison of IPMSMs with unsymmetrical double-layer windings. In Proceedings of the 2017 Twelfth International Conference on Ecological Vehicles and Renewable Energies (EVER), Monte Carlo, Monaco, 11–13 April 2017; pp. 1–6.
8. Wi, C.H.; Lim, D.K. Tornado Optimization with Pattern Search Method for Optimal Design of IPMSM. *IEEE Trans. Magn.* **2022**, *58*, 1–4. [[CrossRef](#)]
9. Venter, G. *Review of Optimization Techniques*; John Wiley & Sons Ltd.: Hoboken, NJ, USA, 2010.
10. Lee, T.-Y.; Trung, P.X.; Kim, J.-W.; Kim, Y.-J.; Jung, S.-Y. Search Region Management Method for Local Search Algorithm Employing Design Optimization of Brushless DC Motor. *IEEE Trans. Magn.* **2016**, *52*, 8200606. [[CrossRef](#)]
11. Song, Z.; Liu, C. Electric Machine Design by a Novel Fast Model Predictive Optimization Strategy Treating Dimension-Expensive Problem. *IEEE Trans. Transp. Electrif.* **2022**, *9*, 2683–2692. [[CrossRef](#)]
12. Yu, H.; Chung, C.Y.; Wong, K.P.; Lee, H.W.; Zhang, J.H. Probabilistic Load Flow Evaluation with Hybrid Latin Hypercube Sampling and Cholesky Decomposition. *IEEE Trans. Power Syst.* **2009**, *24*, 661–667. [[CrossRef](#)]
13. Ullah, K.; Jiang, Q.; Geng, G.; Rahim, S.; Khan, R.A. Optimal Power Sharing in Microgrids Using the Artificial Bee Colony Algorithm. *Energies* **2022**, *15*, 1067. [[CrossRef](#)]
14. Wang, L.; Zhang, X.; Zhang, X. Antenna Array Design by Artificial Bee Colony Algorithm with Similarity Induced Search Method. *IEEE Trans. Magn.* **2019**, *55*, 1–4. [[CrossRef](#)]
15. Bishop, C.M. *Pattern Recognition and Machine Learning*; Springer: Berlin/Heidelberg, Germany, 2006.
16. Cristianini, N.; Shawe-Taylor, J. *An Introduction to Support Vector Machines and Other Kernel-Based Learning Methods*; Cambridge University Press: Cambridge, UK, 2000.
17. Lu, H.; Guo, W.; Su, C.; Li, X.; Lu, Y.; Chen, Z.; Zhu, L. Optimization on Adhesive Stamp Mass-Transfer of Micro-LEDs With Support Vector Machine Model. *IEEE J. Electron Devices Soc.* **2020**, *8*, 554–558. [[CrossRef](#)]
18. Nelder, J.A.; Mead, R. A Simplex Method for Function Minimization. *Comput. J.* **1965**, *7*, 308–313. [[CrossRef](#)]
19. Luersen, M.A.; Le Riche, R. Globalized Nelder–Mead method for engineering optimization. *Comput. Struct.* **2004**, *82*, 2251–2260. [[CrossRef](#)]
20. Chen, C.; Yu, L. A Hybrid Ant Lion Optimizer with Improved Nelder–Mead Algorithm for Structural Damage Detection by Improving Weighted Trace Lasso Regularization. *Adv. Struct. Eng.* **2020**, *23*, 468–484. [[CrossRef](#)]
21. Wan, X.; Yang, S.; Li, Y.; Shi, Y.; Lou, J. Minimization of Cogging Torque for V-Type IPMSM by the Asymmetric Auxiliary Slots on the Rotor. *IEEE Access* **2022**, *10*, 89428–89436. [[CrossRef](#)]
22. Lee, J.H. The Development of Particle Swarm Optimization Based on Intelligent Particle Number Control Method and Optimal Design of EV Traction Motor. Ph.D. Thesis, Sungkyunkwan University, Seoul, Republic of Korea, 2018.
23. Chi, S.; Yan, J.; Guo, J.; Zhang, Y. Analysis of Mechanical Stress and Vibration Reduction of High-Speed Linear Motors for Electromagnetic Launch System. *IEEE Trans. Ind. Appl.* **2022**, *58*, 7226–7240. [[CrossRef](#)]
24. Yamazaki, K.; Aoki, A. 3-D Electromagnetic Field Analysis Combined with Mechanical Stress Analysis for Interior Permanent Magnet Synchronous Motors. *IEEE Trans. Magn.* **2016**, *52*, 1–4. [[CrossRef](#)]
25. Zhou, P.; Lin, D.; Xiao, Y.; Lambert, N.; Rahman, M.A. Temperature-Dependent Demagnetization Model of Permanent Magnets for Finite Element Analysis. *IEEE Trans. Magn.* **2012**, *48*, 1031–1034. [[CrossRef](#)]
26. Kim, K.C.; Kim, K.; Kim, H.J.; Lee, J. Demagnetization Analysis of Permanent Magnets According to Rotor Types of Interior Permanent Magnet Synchronous Motor. *IEEE Trans. Magn.* **2009**, *45*, 2799–2802.
27. Chai, F.; Li, Y.; Liang, P.; Pei, Y. Calculation of the Maximum Mechanical Stress on the Rotor of Interior Permanent-Magnet Synchronous Motors. *IEEE Trans. Ind. Electron.* **2016**, *63*, 3420–3432. [[CrossRef](#)]

Disclaimer/Publisher’s Note: The statements, opinions and data contained in all publications are solely those of the individual author(s) and contributor(s) and not of MDPI and/or the editor(s). MDPI and/or the editor(s) disclaim responsibility for any injury to people or property resulting from any ideas, methods, instructions or products referred to in the content.